JOURNAL OF CATALYSIS 141, 34–47 (1993)

# Magnesia-Supported Nickel Catalysts

## II. Surface Properties and Reactivity in Methane Steam Reforming

A. PARMALIANA,*[1] F. ARENA,† F. FRUSTERI,† S. COLUCCIA,‡ L. MARCHESE,‡ G. MARTRA,‡ AND A. L. CHUVILIN§

*Dipartimento di Chimica Industriale, Università degli Studi di Messina, Salita Sperone c.p. 29, I-98166 S. Agata (Messina), Italy; †Istituto CNR-TAE, Salita S. Lucia 39, I-98126 S. Lucia (Messina), Italy; ‡Dipartimento di Chimica Inorganica, Chimica Fisica e Chimica dei Materiali, Università degli Studi di Torino, Via P. Giuria 7, I-10125 Torino, Italy; §Institute of Catalysis, Prospekt Akademika Lavrentieva 5, 630090 Novosibirsk, Russia

Received April 15, 1992; revised July 23, 1992

Surface properties and reactivity of Ni/MgO catalysts, air-calcined at temperatures ($T_C$) in the range 400–800°C, have been evaluated by TEM, IR spectroscopy of adsorbed CO, and catalytic measurements in methane steam reforming. The effects of calcination and reduction temperature on the Ni particle size distribution (PSD) provide evidence of the singular structure properties of the Ni/MgO system. The "broad" PSD of samples calcined at $T_C \leq 600$°C well accounts for the structure model previously described (Arena, F., Horrell, B. A., Cocke, D. L., Parmaliana, A., and Giordano, N., *J. Catal.* **132,** 58 (1991)). IR spectroscopy shows both the formation of mono- and polycarbonyls and the occurrence of the CO disproportionation reaction ($2\ CO \rightleftharpoons CO_2 + C$). The higher reactivity towards CO of more dispersed systems has been attributed to the "defective nature" of small Ni crystallites. Catalytic measurements ($T_R = 625$°C; GHSV = 150,000 $h^{-1}$) reveal the superior activity of the system calcined at $T_C = 400$°C, notwithstanding that a comparable stability for the systems calcined up to 600°C has been experienced. At higher $T_C$ (>600°C) the catalytic pattern, both in terms of activity and resistance to coking, is negatively affected by the formation of the "bulk" NiO–MgO solid solution. The peculiar influence of the mean Ni particle size ($20 \leq d_s \leq 1400$ Å) on the turnover frequency (TOF, $s^{-1}$), resulting in a volcano-shape relationship with the maximum centred at 90–130 Å, has been explained by invoking a structure-sensitive character of the methane stream-reforming reaction on highly dispersed Ni/MgO catalysts. 

### INTRODUCTION

Despite the large number of studies focused on the surface characterization of the Ni/MgO system (*1–9*), including those dealing with the physico-chemical properties of NiO–MgO solid solutions (*2–4*, *8*), there are comparatively few investigations devoted to elucidating its catalytic behaviour (*2*, *6*, *9*). A significant effort has been made to ascertain the influence of the preparation method on the structure and surface properties of Ni/MgO (*1*, *10–13*). It is generally accepted that its reactivity is markedly affected by the propensity to form NiO–MgO solid solutions (*2*, *4*, *6*, *9*, *14*). The effects of the calcination temperature ($T_C$) and of the Ni loading on the structure and morphology of the NiO/MgO system have been the subject of our previous investigations (*1*, *11*). In particular, the substantial changes in metal dispersion and NiO reducibility with $T_C$ have been rationalised by means of a solid-state reaction model involving the diffusion of $Ni^{2+}$ ions across the MgO lattice which leads to the formation of a substitutional and nonreducible NiO–MgO solid solution (*1*).

The addition of magnesia exerts a positive effect on the performance of typical Ni-

[1] To whom correspondence should be addressed.



0021-9517/93 $5.00

based steam reforming catalysts, lowering the coking rate (*2*) and enhancing the mechanical strength (*15*). The basic nature of the magnesia surface appears to be crucial in hindering the coking effects caused by direct cracking of hydrocarbons (*16*). Moreover, Borowiecki emphasised the influence of calcination and reduction temperatures in stabilising a surface MgO-rich phase which improves the capability of the Ni/MgO catalyst for steam adsorption, thereby allowing a higher gasification rate of carbonaceous deposits (*2*). In spite of this, the use of MgO as support in "working catalysts" has until now been limited by its poor stability (*17*) and the negative effect on the NiO reducibility which depresses the development of high active metal areas (*1*, *18*). Nevertheless, these problems have been overcome by adopting a novel preparation method based on the incipient wetness of *smoke* MgO as the carrier, with high thermal stability (*19*), and by selecting adequate Ni loading (>11%) and thermal treatments which enable low extents of NiO–MgO solid solutions (*1*) allowing then a considerable performance in $CH_4$ steam reforming (*9*).

This study attempts to point out a systematic correlation between the surface properties and the catalytic pattern in $CH_4$ steam reforming of a "real" 18 wt% Ni/MgO catalyst. TEM and IR spectroscopy were used to monitor the influence of activation treatments (i.e., calcination and reduction) on the morphology and reactivity of supported Ni crystallites.

## EXPERIMENTAL

### *Catalyst*

Supported nickel on magnesia catalysts were prepared by the incipient wetness method according to the procedure described elsewhere (*11*). The influence of the calcination temperature on surface and catalytic properties has been evaluated by calcining in an air flow for 16 h several aliquots of a dried 18 wt% Ni/MgO sample (MPF 12) at 400°C (MPF 12-std), 600°C (MPF 12-6), and 800°C (MPF 12-8).

### *TEM Analysis*

The morphology and the size distribution of Ni particles were determined by a JEOL 100 C transmission electron microscope (point-to-point resolution, 5 Å) using a finely ground and ultrasonically dispersed (in ethanol) catalyst sample deposited on a thin carbon film supported on a standard copper grid. Prior to TEM measurements nickel catalysts were reduced in flowing $H_2$ for half an hour at temperatures ($T_r$) ranging between 400 and 800°C. To estimate the mean particle size, the normal statistical formulae (*20*) were used by considering at least ca. 500 particles for each catalyst sample.

### *Infrared Spectroscopy*

Self-supporting pellets of the catalyst were placed into IR cells permanently connected to vacuum lines (residual pressure $\approx 10^{-6}$ Torr; 1 Torr = 133 Pa) which allowed all reduction pretreatments and adsorption–desorption experiments to be carried out *in situ*.

Before CO admission the pellets were reduced at $T_r$ ranging between 400 and 800°C, then outgassed at the same temperature for half an hour. High purity gases (Matheson) were used with no further purification except liquid nitrogen trapping.

CO adsorption experiments were performed at room temperature and IR spectra were obtained using Bruker IFS 113V and IFS 48 instruments. The resolution was 4 $cm^{-1}$. The IR spectra of adsorbed CO in the range 2200–1200 $cm^{-1}$ are reported on an absorbance scale after subtraction of background spectra.

### *Catalytic Tests*

The activity and stability of Ni/MgO catalyst in methane steam reforming reaction have been evaluated by a continuous flow fixed-bed quartz microreactor ($l$ = 200 mm; i.d. = 4 mm) operating at atmospheric pressure. Nitrogen, used as internal standard (for GC), and methane (SIO product, purity >99.5%) were bubbled together ($P_{CH_4}/P_{N_2}$ equal to 10/1) into a thermostatically con-

trolled $H_2O$ saturator kept at 90°C (±0.01°C) so as to have a fixed ratio $P_{H_2O}/P_{CH_4}$ equal to 2.54/1. The reaction mixture was fed into the reactor containing the catalyst ($W_{cat}$ = 0.02 g; 40–70 mesh) diluted with same-sized carborundum (1/10, vol/vol) to ensure quasi-ideal conditions for mass and heat transfer. Reactants and reaction products were analysed by on-line GC (9). Prior to each test the catalyst was reduced *in situ* ($400 \leq T_r \leq 1000$°C) under hydrogen flow (50 STP ml $min^{-1}$) for half an hour, then conditioned to reaction temperature ($T_R$) in the He atmosphere. Measurements were performed in the $T_R$ range 600–650°C with space velocity (GHSV, $h^{-1}$) ranging from 75,000 to 300,000 $h^{-1}$. The extent of methane conversion (mol%) was taken as a measure of the catalytic activity. In order to obtain reliable turnover frequency (TOF, $s^{-1}$) data, a series of experiments in differential conditions were carried out at $T_R$ ranging between 430 and 600°C with the above MPF 12 samples and differently loaded Ni/MgO catalysts (MPF 13-std, MPF 15-std and PM series) [see Ref. (*1*) for the preparation method and physico-chemical properties].

## RESULTS

### *Transmission Electron Microscopy (TEM)*

Differently air-calcined MPF 12 samples have been characterised by TEM in order to achieve direct information on the morphology and Ni particle size distributions (PSD).

Representative TEM micrographs of MPF 12 catalysts reduced at 600 and 800°C are shown in Fig. 1. It is immediately evident that the "cubic" structure of the "smoke" MgO is substantially unaffected by the preparation procedure in samples calcined at $T_C \leq 600$°C (Figs. 1a, a', b, b'), whereas at $T_C$ = 800°C (Figs. 1c, c') a remarkable sintering affects both the size and the regular morphology of the support particles. In addition, for the MPF 12-std and MPF 12-6 samples a large amount of Ni crystallites, mainly located on the most defective positions of the MgO structure (i.e., edges, corners), is easily distinguishable from the "open" structure of the support. In particular, the Ni particles of MPF 12-std and MPF 12-6 samples reduced at 600°C appear to be slightly "pulled" and "sunk" in the MgO structure (Fig. 1a, b), while upon reduction at 800°C (Fig. 1a', b') they outcrop more distinctly from the support becoming more regular-shaped thereby rendering the Ni/MgO system more similar to a conventional supported system.

By contrast, MPF 12-8 catalyst reduced at 600°C (Fig. 1c) is very difficult to analyse because of either the low percentage of reduced NiO or insufficient contrast between the small nickel crystallites (<20 Å) and the support (*1*), while the reduction at 800°C (Fig. 1c') allows the formation of larger Ni particles, the morphology of which is similar to that already observed for MPF 12-std and MPF 12-6 samples reduced at 600°C.

In Fig. 2 are shown the particle size distributions (PSD) of the MPF 12 catalysts reduced at 600 and 800°C. The MPF 12-std and MPF 12-6 samples reduced at 600°C (Figs. 2a and b) present a similar broad PSD, spanned in the range 25–125 Å, with a prevailing contribution of small Ni particles ($d$ < 75 Å). However, a larger percentage of Ni particles with $d$ = 25 Å is clearly observable for the MPF 12-std catalyst (Fig. 2a). At $T_r$ = 800°C (Fig. 2a', b'), we note a further broadening in the PSD ($25 \leq d \leq 200$ Å) involving a greater contribution of Ni particles with $d > 75$ Å and a lowering in the fraction of Ni particles with $d$ = 25 Å. Both such effects are more evident for the MPF 12-std sample (Fig. 2a').

The PSD's of the MPF 12-8 (Figs. 2c and c') sample appear to be notably narrower (25–75 Å) than those previously considered for MPF 12-std and MPF 12-6 catalysts. In particular, at $T_r$ = 600°C (Fig. 2c) there is a remarkable contribution of the Ni particles with $d$ = 25 Å (≈70%) which slightly lowers (≈55%) at $T_r$ = 800°C (Fig. 2c').

Additionally, we found that the values of surface average Ni particle size ($d_s$) (*20*), estimated by TEM analysis, are in ex-

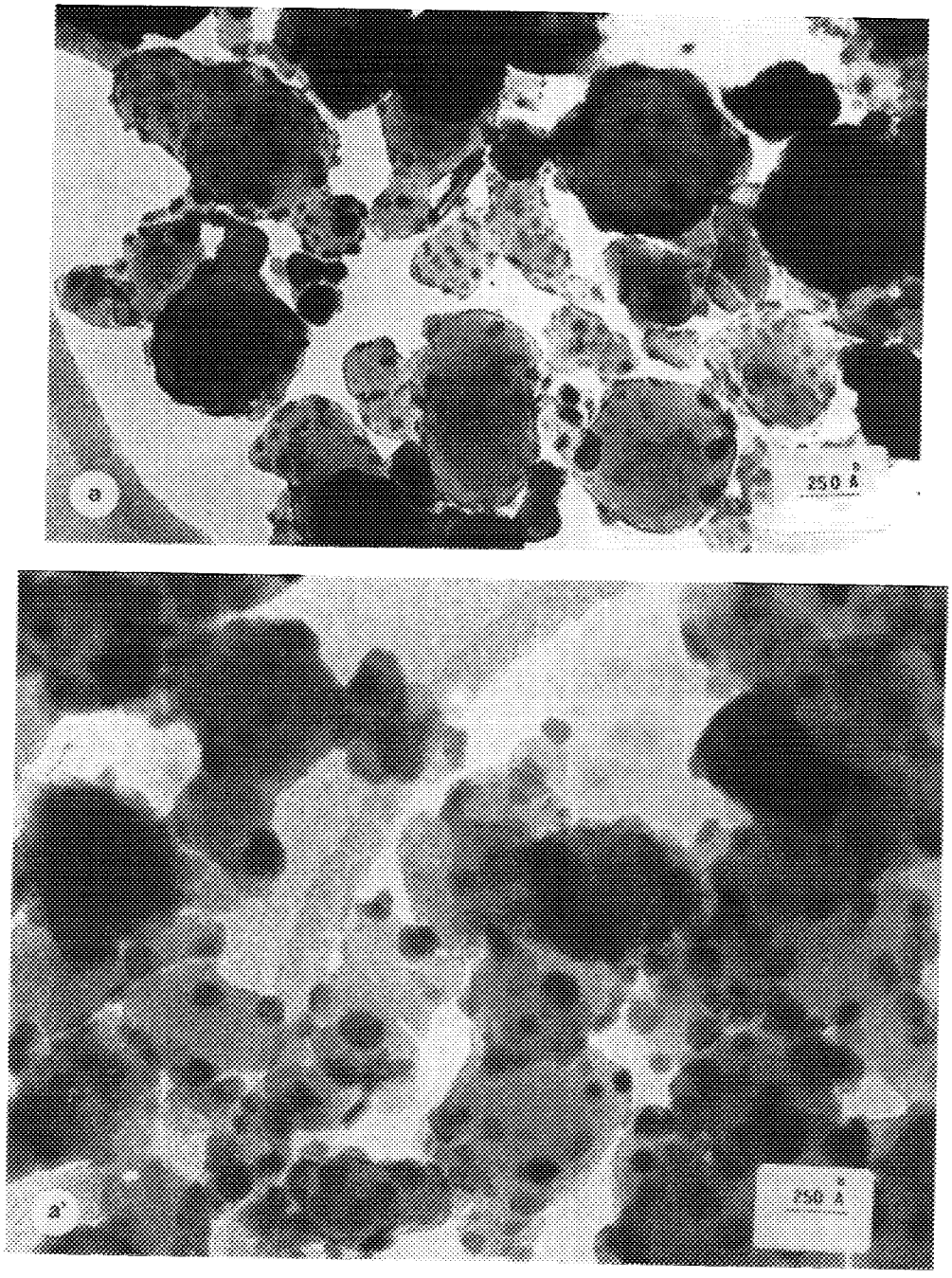


FIG. 1. TEM micrographs of MPF 12-std (a, a'), MPF 12-6 (b, b'), and MPF 12-8 (c, c') catalysts reduced at 600 (a, b, c) and 800°C (a', b', c') respectively.

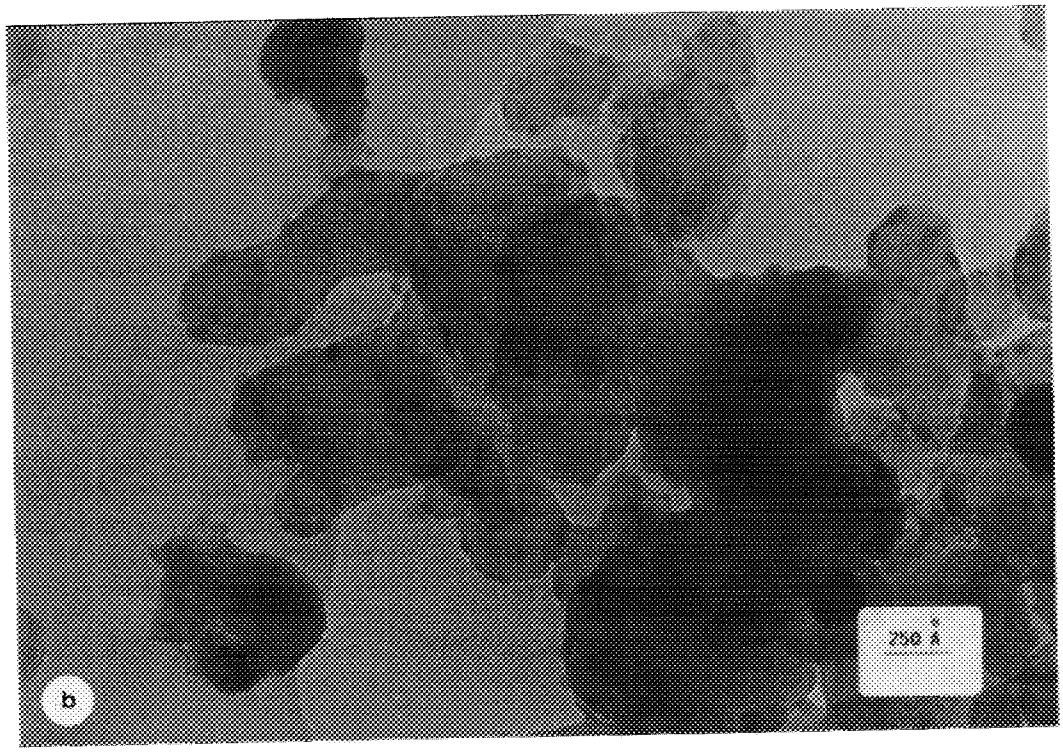


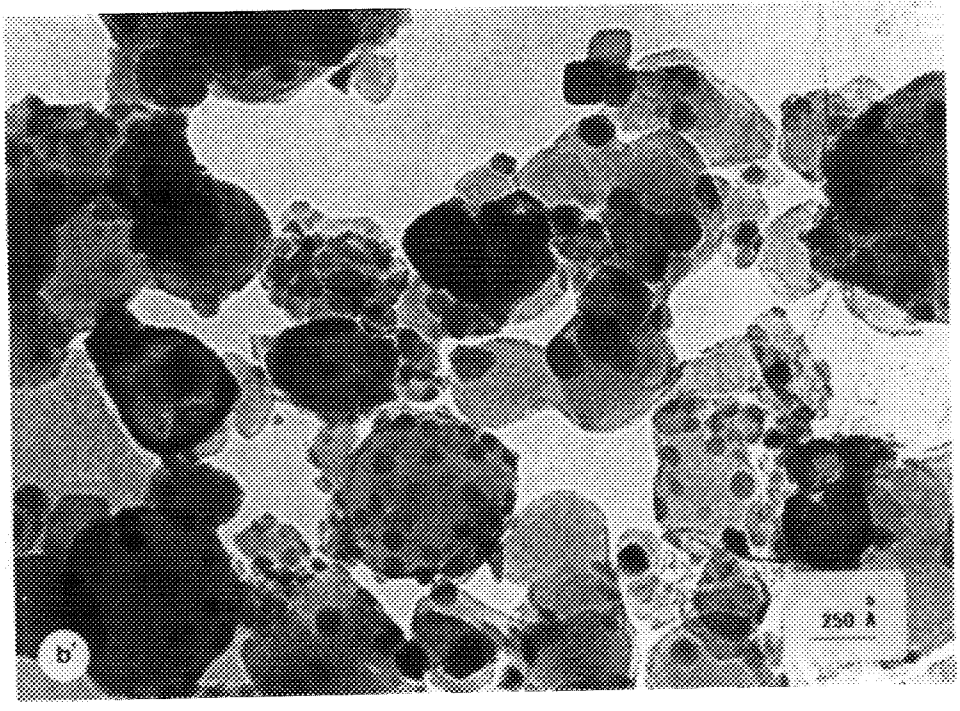


FIG. 1—*Continued*

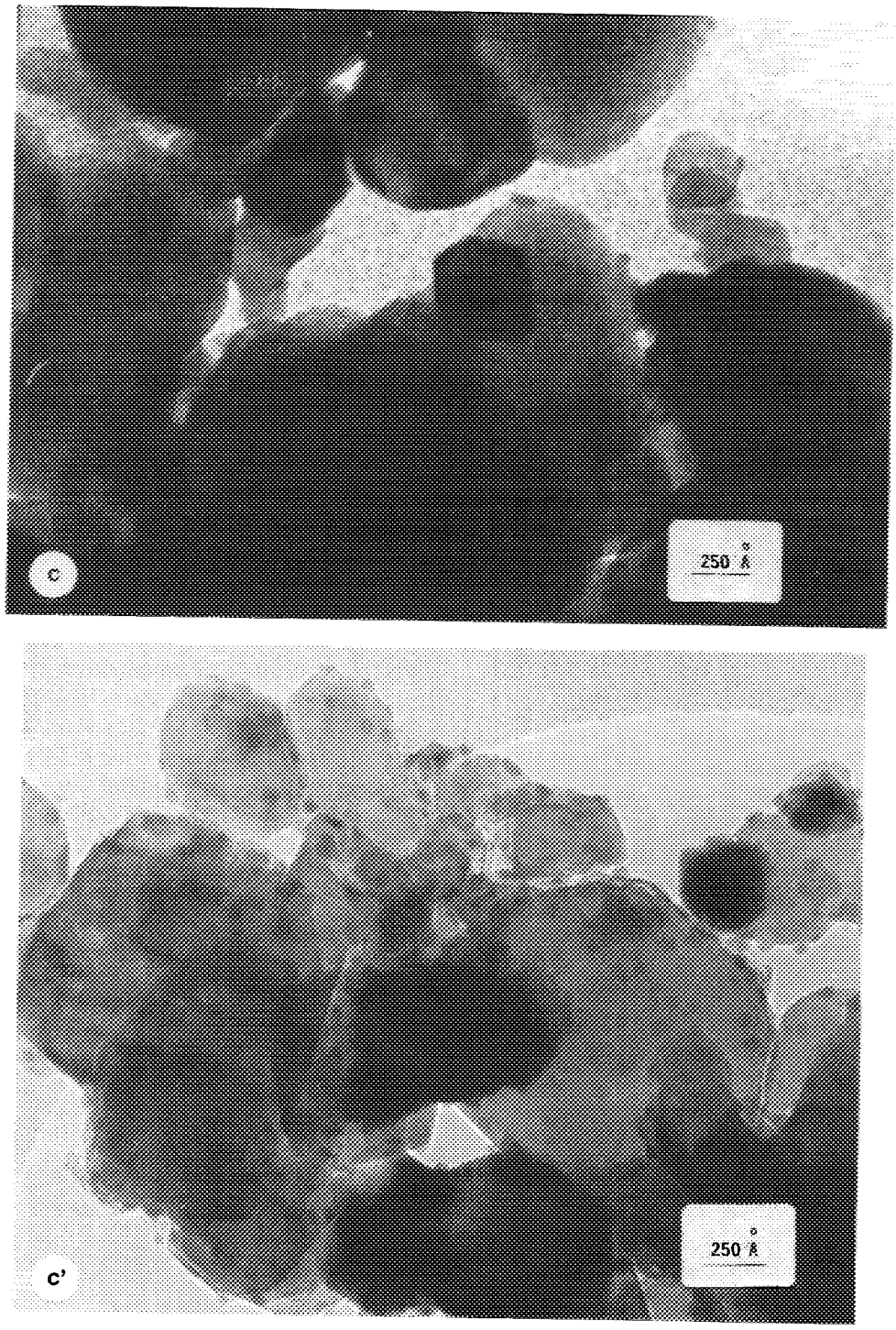


FIG. 1—*Continued*

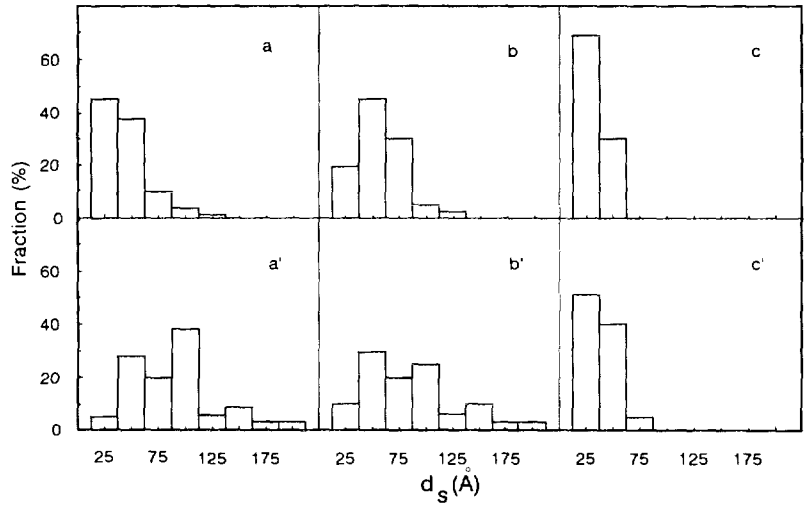


FIG. 2. Particle size distribution of MPF 12-std (a, a'), MPF 12-6 (b, b'), and MPF 12-8 (c, c') catalysts reduced at 600 (a, b, c) and 800°C (a', b', c'), respectively.

cellent agreement with those calculated by hydrogen chemisorption (*1*) as shown in Table 1.

*IR Spectroscopy*

The spectra of CO adsorbed under low gas pressure ($P_{CO} \approx 0.2$ torr) on the MPF 12 catalysts, previously reduced at 600°C, are shown in Fig. 3. For the sake of clarity the results will be described separately for range A (2200–1800 $cm^{-1}$) and range B (1800–1200 $cm^{-1}$).

*Range A (2200–1800 $cm^{-1}$).* Two broad bands are present with maxima at 2060 and 1965 $cm^{-1}$, strongly asymmetric on the low-frequency side. The spectrum of the MPF 12-6 catalyst (curve b) exhibits shoulders at 2045 and 1935 $cm^{-1}$, while for MPF 12-std sample (curve a) a shoulder appears at $\approx$1910 $cm^{-1}$. By increasing $T_C$, the intensity of the peaks decreases (curves a–c); the band at $\approx$1965 $cm^{-1}$ is more sensitive to this

TABLE 1

Characterization of Ni/MgO Catalysts

| Catalyst | Reduction temperature (°C) | Extent of reduction (%) | Particle size | |
|---|---|---|---|---|
| | | | $d_{s(chem)}$[1] (Å) | $d_{s(TEM)}$ (Å) |
| MPF 12-std | 600 | 47.3 | 66 | 66 |
| MPF 12-std | 800 | 76.5 | 107 | 107 |
| MPF 12-6 | 600 | 32.0 | 87 | 70 |
| MPF 12-6 | 800 | 62.0 | 128 | 114 |
| MPF 12-8 | 600 | 2.6 | 26 | — |
| MPF 12-8 | 800 | 11.2 | 43 | 49 |

[1] Values derived from Ref. (*1*).

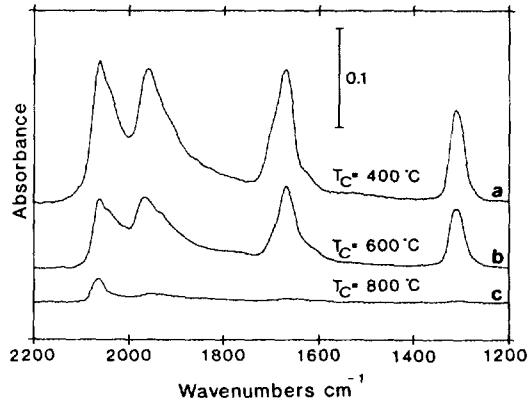


FIG. 3. IR spectra of CO adsorbed on MPF 12-std (a), MPF 12-6 (b), and MPF 12-8 (c) catalysts reduced at 600°C.

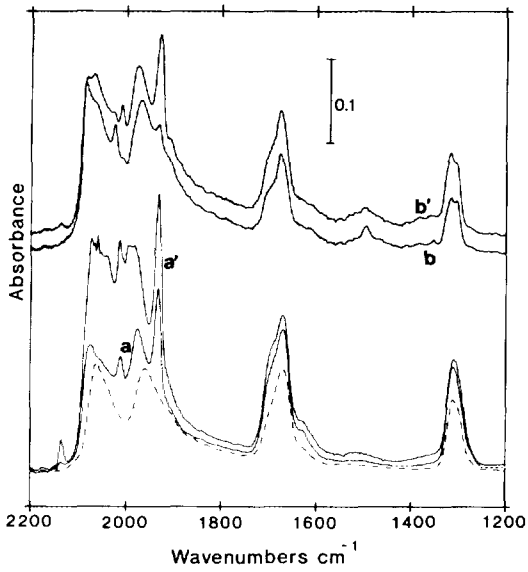


FIG. 4. IR spectra of CO adsorbed on MPF 12-std catalyst reduced at 600 (a, a') and 800°C (b, b') immediately after admission of 10 Torr CO (a, b) and after 1 h of contact (a', b'). For comparison the spectrum of MPF 12-std catalyst reduced at 600°C under low CO pressure is shown (---).

effect, being nearly absent for $T_C$ = 800°C (curve c).

*Range B (1800–1200 cm$^{-1}$).* In this range two bands are observed at 1670 and 1310 cm$^{-1}$. Both bands decrease in intensity with increasing $T_C$ (curves a–c), becoming nearly undetectable for the MPF 12-8 catalyst (curve c). Their dependence on pressure and time of contact with CO (spectra not reported) shows that they are related to each other.

Figure 4 shows the influence of $T_r$ (600 and 800°C) and time of contact on the spectra of CO adsorbed on the MPF 12-std catalyst. The spectra were recorded immediately after adsorption of 10 Torr CO (curves a and b) and after allowing 1 hour of contact under such CO pressure (curves a' and b'). For comparison also the spectrum of CO adsorbed under low gas pressure on the MPF 12-std catalyst reduced at 600°C is reported (dashed line).

*Range A (2200–1800 cm$^{-1}$).* The spectrum recorded immediately after admission of 10 Torr CO to the sample reduced at 600°C (curve a) shows the bands already present at low CO pressure (cf. dashed line), although slightly more intense and shifted to higher frequencies, and two narrow peaks at 2010 and 1930 cm$^{-1}$. A prolonged time of contact with CO (curve a') involves a considerable increase in the overall intensity of the bands and the appearance of new peaks at 2136, 2070, 2035, and 2000 cm$^{-1}$.

The intensity of the spectrum obtained immediately after admission of CO to the sample reduced at 800°C (curve b) is similar to that of the sample reduced at 600°C (curve a). However, two new peaks appear at 2085 and 2025 cm$^{-1}$, while the intensity of the bands at 2010 and 1930 cm$^{-1}$ is decreased. Furthermore, it is noteworthy that the effects of prolonged contact of CO with the two samples are greatly different, being less effective for that reduced at higher temperature. In fact, upon 1 h of exposure to CO (curve b') the overall intensity of the spectrum of the sample reduced at 800°C does not change significantly, although some decrease in intensity of the bands at 2085 and 2025 cm$^{-1}$ and the increase of the couple at 2010 and 1930 cm$^{-1}$ are observed.

*Range B (1800–1200 cm$^{-1}$).* The IR absorption in this range looks similar to that presented in Fig. 3 resulting in two main bands at 1670 and 1310 cm$^{-1}$. These bands grow with the CO pressure whereas they are not significantly affected by prolonged exposure of the samples to CO nor by $T_r$ (curves a' and b').

Another band centred at 1500 cm$^{-1}$ is present on the sample reduced at 800°C immediately after adsorption of CO (curve b). It disappears after long time of contact (curve b') and is very weak on the sample reduced at 600°C.

### *Catalytic Activity Measurements*

Preliminary experiments dealing with the influence of the space velocity on the activity and stability of MPF 12-std catalyst in the $T_R$ range 600–650°C showed that GHSV

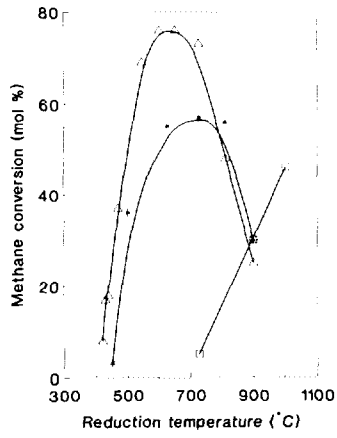


FIG. 5. Effect of the reduction temperature ($T_r$) on the catalytic activity of (△) MPF 12-std, (*) MPF 12-6, and (□) MPF 12-8 catalysts in methane steam reforming. $T_R$ = 625°C, $P_{H_2O}/P_{CH_4}$ = 2.54; GHSV = 150,000 $h^{-1}$.

higher than 75,000 $h^{-1}$ might be adopted to avoid the constraints imposed by the thermodynamic equilibrium (9). Therefore, in order to find out how the calcination and reduction treatments influence the activity and stability of MPF 12 catalysts, a series of experiments has been performed at $T_R$ = 625°C and GHSV = 150,000 $h^{-1}$.

Integral measurements indicate that the catalytic activity of differently air-calcined MPF 12 catalysts, expressed as percentage $CH_4$ conversion (mol %), is markedly affected by $T_r$, as shown in Fig. 5. For MPF 12-std and MPF 12-6 samples it results in a volcano-shape relationship whose maximum shifts to higher $T_r$ with $T_C$, whereas for the MPF 12-8 sample only a slight increasing activity is observed at $T_r \geq 725$°C. However, the MPF 12-std catalyst ($T_C$ = 400°C) exhibits in any case a superior reactivity with respect to systems calcined at higher $T_C$ (MPF 12-6 and MPF 12-8). Furthermore, in Fig. 6 is compared the stability of MPF 12 catalysts, previously reduced at 725°C, in terms of relative activity, $a$, ($a = a_t/a_0$, where $a_t$ and $a_0$ are respectively the activity at time $t$ and at 0.5 h) versus the reaction time. It is notable that at GHSV of 100,000 $h^{-1}$ MPF 12-std and MPF 12-6 catalysts show an excellent stability, while at 150,000 $h^{-1}$ there is a similar slight decrease in their activities, although MPF 12-6 catalyst on the whole appears more stable. MPF 12-8 catalyst behaves differently, showing a sudden drop in activity which leads to a complete deactivation after ca. 15 h and 20 h at a space velocity of 150,000 and 100,000 $h^{-1}$, respectively.

In order to probe the influence of the Ni particle size on the reactivity of Ni/MgO catalysts a series of catalytic tests in differential conditions ($CH_4$ conv. < 8 mol %), suitable for turnover frequency (TOF, $s^{-1}$) calculations, has been performed in the $T_R$ range 430–600°C on samples with $d_s$ ranging from 20 to 1400 Å (1). A peculiar relationship between TOF and $d_s$, obtained at $T_R$ = 430°C, is shown in Fig. 7. It presents a broad maximum between 90 and 130 Å. In particular, for $d_s$ increasing from 20 to 90 Å, the TOF suddenly increases from 0.01 to 0.61 $s^{-1}$; thereafter (130 < $d_s$ < 400 Å) it gradually slows, ultimately reaching a constant value of 0.25 $s^{-1}$ (400 < $d_s$ < 1400 Å). Furthermore, in Table 2 are summarized several representative TOF values at various $T_R$ for Ni/MgO catalysts with different $d_s$. These data confirm the trend observed at 430°C, undoubtedly proving the critical influence exerted by Ni particle size on the specific activity of Ni/MgO catalysts.

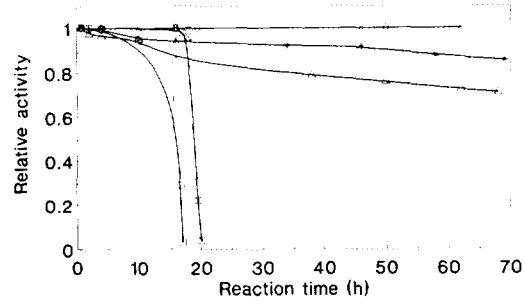


FIG. 6. Stability tests of MPF 12-std (◇, △), MPF 12-6 (×, *), and MPF 12-8 (⧖, □) catalysts in methane steam reforming. $T_R$ = 625°C; $P_{H_2O}/P_{CH_4}$ = 2.54; GHSV = 100,000 (◇, ×, ⧖) and 150,000 $h^{-1}$ (△, *, □).

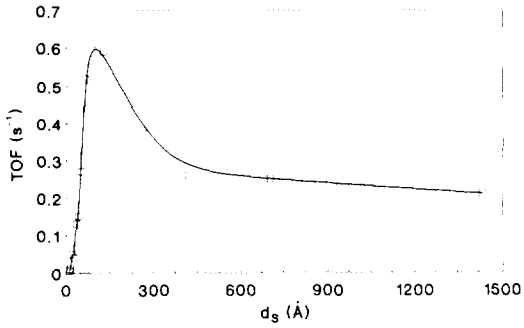


FIG. 7. Influence of the surface average Ni particle size ($d_s$) on the turnover frequency (TOF) for methane steam reforming on Ni/MgO catalysts. $T_R$ = 430°C; $P_{H_2O}/P_{CH_4}$ = 2.54.

## DISCUSSION

### 1. *Influence of Calcination and Reduction Treatments on the Morphology of Ni/MgO Catalysts*

*Transmission electron microscopy.* The "wide" dispersity of NiO across the MgO matrix, regulated by $T_C$, accounts for the different reducibility of several "NiO forms" (*11*) and the morphology of the resulting Ni crystallites (*1*). In this respect, the formation of Ni particles partially sunk in the MgO lattice and with irregular morphology (plate-like and faceted particles) is a direct evidence of the singular interaction mechanism between NiO and MgO involving their reciprocal *intermixing* (*1, 3*). Also the broad PSD's of MPF 12-std and MPF 12-6 systems, shown in Fig. 2 a–a′ and b–b′, further support our view on the structural features of the Ni/MgO system (*1*). It can be inferred that on these samples the $H_2$ treatment at 600°C gives rise both to an incipient sintering of Ni particles arising from the easily reducible "free" NiO form (*11*) and to a concomitant and continuous reduction of $Ni^{2+}$ ions "anchored" on the surface sites and in the sub-surface layers of the MgO matrix (*11*). Both these processes well explain the formation of differently sized Ni particles (Fig. 2a, b). However, the PSD of the MPF 12-6 sample displays a lower contribution of the small Ni particles ($d$ = 25 Å) which can be related with the less effective reduction of the surface NiO–MgO solid solution (*12*). Clearly, a rise in $T_r$ from 600 to 800°C results in a further broadening of the PSDs (see Fig. 2a′, b′) and in an enhanced sintering rate which causes a significant shift of $d_s$ to higher values (see Table 1).

Therefore, although the calcination at 600°C leads to a growth of $d_s$ as a consequence of the NiO sintering (*1*), the similar PSD's of MPF 12-std and MPF 12-6 samples reflect rather a significant similarity in their morphological properties (*1*). On the other hand, a further rise in $T_C$ from 600 to 800°C causes a deep structural rearrangement linked with the formation of a "bulk" NiO–MgO solid solution (*12*), the reduction of which, proceeding by the *extraction* of $Ni^{2+}$ ions from the MgO matrix (*1*), leads to highly dispersed systems (Fig. 2c, c′).

*Infrared spectroscopy of adsorbed CO.* The progressive decrease in the integral intensity of IR spectra of adsorbed CO (Fig. 3) appears as a confirmatory evidence of the increasing resistance to reduction of the Ni/MgO catalysts calcined at higher $T_C$ and consequently of their lower metal surface area (MSA, $m^2_{Ni}\, g^{-1}_{cat}$) (*1*). In particular, these spectra present two main IR absorptions centered at 2060 and 1965 $cm^{-1}$, respectively assigned to linear and bridged carbonyls (*21–29*). Their broadness and complexity reflect the surface heterogeneity of Ni particles accommodating sites with different coordination on microfaces, edges and corners. It is generally accepted that CO molecules in bridged carbonyls may be coordinated to two or three $Ni^0$ atoms (*21, 22, 24, 25, 28*) and in our case threefold coordinated CO species may well be responsible for the shoulder on the low frequency side of the main peak at 1965 $cm^{-1}$. However, bridged carbonyls are preferentially formed on the faces of the metal particles where sets of $Ni^0$ atoms with the required geometry may be found (*22*). Consequently, the formation of such species should be favoured on large particles (*24, 28*) and this

TABLE 2

Turnover Frequencies (TOF) on Ni/MgO Catalysts in Methane Steam Reforming at Different Reaction Temperatures ($T_R$)

| Sample | $T_r$ (°C) | $d_{s(chem)}$[1] (Å) | | TOF ($s^{-1}$) | | |
|---|---|---|---|---|---|---|
| | | | $T_R$(°C): | 430 | 500 | 600 |
| MPF 13-std | 800 | 34 | | 0.13 | 1.1 | 2.6 |
| MPF 12-std | 725 | 90 | | 0.61 | 1.8 | 4.9 |
| PM-std | 400 | 694 | | 0.23 | 1.2 | 2.7 |

[1] $d_s$ values derived from Ref. (*1*).

agrees well with the fact that the absorption at 1965 $cm^{-1}$ is extremely weak in the spectrum of the MPF 12-8 sample (Fig. 3c) characterised by the smallest average Ni particle size (Table 1). Indeed, it should be noticed that on this system, resulting from the reduction of a proper solid solution (*1*, *11*), the contribution of "atomically dispersed" $Ni^0$ clusters might be even larger than that expected on the basis of hydrogen chemisorption data (*1*) and TEM analysis.

The bands at 1670 and 1310 $cm^{-1}$ (Fig. 3) are diagnostic of surface carbonate-like groups (*30*) originated by the Boudouard reaction,

$$2\ CO \rightleftharpoons CO_2 + C,$$

and the consequent adsorption of $CO_2$ formed on $O^{2-}$ ions of the MgO surface (*31*). Thus, the appearance of carbonate groups on MPF 12-std and MPF 12-6 catalysts monitors the existence of Ni sites able to dissociate the carbon monoxide, promoting meanwhile its further oxidation. By contrast, the very weak intensity of these bands on the spectrum of the MPF 12-8 sample indicates that the Boudouard reaction is strongly inhibited on small Ni particles according to the observation of Galuska *et al.* (*32*).

Further details on the morphology of supported Ni particles can be obtained from the IR spectra presented in Fig. 4. Namely, we note that these spectra in range A are characterised by the overlapping of several bands associated with the formation of polycarbonyl species (*33*, *34*). The intensity of such bands increases with time, denoting that these species arise from the disruption of metal particles by an activated process similar to that described in detail for Mo-containing catalysts (*35*). It was argued that metal atoms exposed on sites with the lowest coordination (corners, edges and steps, etc.) are more easily attacked by CO and, consequently, the smallest and roughest particles are disrupted faster (*36*, *37*). This agrees with the observation that time of contact with CO appears to be less effective for the MPF 12-std sample reduced at 800°C (spectra b and b′) than for the sample reduced at 600°C (spectra a and a′). Evidently, the higher complexity of the spectra related to the sample reduced at 600°C indicates the presence of smaller and irregular-shaped Ni particles which sinter, assuming a more regular symmetry, upon $T_r$ increasing to 800°C (Table 1).

### 2. *Influence of Morphological Properties on the Reactivity of Ni/MgO Catalysts in $CH_4$ Steam Reforming*

The influence of the reduction temperature on the reactivity of the MPF 12-std and MPF 12-6 catalysts, shown in Fig. 5, results in a volcano-shape relationship that seems to reflect the trend of metal surface area (MSA) with the percentage NiO reduction ($\alpha$) previously discussed (*1*). This peculiar

effect of $T_r$ on the catalytic activity arises either from its positive influence on the degree of NiO reduction or from the concurrent sintering which negatively affects the development of MSA (*1*). As a consequence of the rise in $T_C$ from 400 to 800°C, the MPF 12 system requires progressively higher $T_r$ to attain its maximum in catalytic activity (Fig. 5) owing to a stronger NiO–MgO interaction which hinders the reduction rate (*11*). The monotonically increasing activity of the MPF 12-8 sample up to 1000°C reflects the predominant effect of $T_r$ on the NiO reduction degree (*11*).

However, even though the highest MSA of the MPF 12-std sample well accounts for its superior activity, on the whole Ni/MgO catalysts display a poor proportionality between the extent of metal active area (*1*) and the level of methane conversion (Fig. 5). Thus the MPF 12-8 catalyst, exhibiting a slight catalytic activity only after reduction at 725°C, shows a significant $H_2$ chemisorption already at $T_r \geq 600$°C (*1*). On the other hand, the MPF 12-6 and MPF 12-8 samples, reduced respectively at 500 and 800°C, present a catalytic activity differing by more than one order of magnitude though their hydrogen uptakes are comparable (*1*). This evidence leads us to infer that the structural properties of the Ni/MgO catalysts exert a critical influence on their reactivity in $CH_4$ steam reforming. In this respect Fig. 7, showing a marked influence of the mean Ni particle size on the TOF value, more adequately highlights the different reactivity of the MPF 12 catalysts. Although this singular trend apparently disagrees with earlier observations claiming a "facile" character for the $CH_4$ steam reforming reaction (*38*), it must be considered that limited attention has hitherto been devoted to Ni-based systems with average Ni particle size lower than 100 Å (*38*). Recently, Che and Bennett (*39*), reviewing the particle size effect for conventional structure-insensitive reactions, pointed out that at high metal dispersion (>50%) both the geometric and the cluster-like electronic effects cause a rapid decrease in TOF to zero. These authors also reported the existence of systems showing a maximum in TOF similar to that presented in Fig. 7. This peculiar behaviour has been attributed to the changes in the composition of the surface and in the related statistical distribution of edges, corners and faces sites with metal dispersion (*40*).

On this account, the unique structural features of the Ni/MgO system, allowing one to span a wide range of metal dispersions, namely, from 90% ($d_s$ = 11 Å, atomic dispersed system) to 0.7% ($d_s$ = 1380 Å, highly sintered system), lead us to disclose that the most dramatic changes in TOF (0.005–0.61 $s^{-1}$) occur in the first region of $d_s$ (<90 Å). These results clearly prove the poor performance of highly dispersed Ni systems, further confirming the unsuitability of NiO–MgO solid solutions as "real" $CH_4$ steam reforming catalysts.

On the whole, our findings can be explained by invoking the occurrence of critical interactions between "adsorbed reaction intermediates" and the metal phase, the strength of which, depending on the morphology of Ni surface, controls the overall reaction rate. In fact, taking into account the high propensity of Ni in promoting the dissociative chemisorption of saturated hydrocarbons (*41*) we attempt to describe our data on the basis of the following reaction mechanism proposed by Agnelli *et al.* (*42*):

$$CH_4 + ns \rightarrow C(s_{n-4}) + 4H(s) \quad (1)$$

$$4H(s) \rightleftharpoons 2H_2 + 4s \quad (2)$$

$$H_2O_a + s \rightleftharpoons H_2 + O(s) \quad (3)$$

$$C(s_{n-4}) + O(s) \rightleftharpoons CO(s) + (n-4)s \quad (4)$$

$$CO(s) \rightleftharpoons CO + s \quad (5)$$

$$CO + O(s) \rightleftharpoons CO_2 + s. \quad (6)$$

Where, $s$, $X(s)$, and $H_2O_a$ refer, respectively, to surface Ni sites, chemisorbed species and $H_2O$ adsorbed on the MgO surface. In particular, according to the evidence already reported for Pt and Pd based systems (*43*, *44*), we infer that the bond between

adsorbed oxygen atoms and Ni sites (O($s$)) has a "structure-sensitive" character resulting more strongly on the highly uncoordinated sites. This interaction probably controls the rate of step (4) in the above reaction pathway. In other words, it can be argued that the recombination of the chemisorbed carbide intermediate (C($s_{n-4}$)) with the O($s$) adatoms, originated from the catalytic decomposition of a water molecule adsorbed on the MgO surface (3) (*14*, *42*), is the rate determining step (r.d.s.). Then, defective Ni sites of low coordination ($d_s < 50$ Å), owing to their stronger interaction with oxygen species, present the lowest TOF values, while the smoothness of large Ni particles, allowing faster transformation of such an intermediate, accounts for higher TOF values. Moreover, the inhibition of the Boudouard reaction on the MPF 12-8 catalyst (Fig. 3), despite the higher decomposition rate of CO observed on small Ni particles (*45*), could also be attributed to a strong Ni–O interaction on this highly dispersed Ni/MgO system.

The different deactivation trends of the MPF 12 catalysts (Fig. 6), resulting mainly in a sudden activity loss of the highly dispersed MPF 12-8 sample, further strengthen the crucial influence of the structural properties on the overall catalytic pattern of the Ni/MgO system. However, in order to rationalize these data we can disregard any negative effect of surface acidity since our previous $CO_2$-TPD results clearly indicated a progressive enhancement in the surface basicity of the Ni/MgO system on increasing $T_C$ from 400 to 1000°C (*46*). Therefore, the only valid argument to explain the different deactivation behaviours of the Ni/MgO catalysts lies in their different metal dispersion. This is well in agreement with the statements of Bartholomew (*47*) indicating that the formation of carbon should be favoured on small Ni particles having a higher frequency of rough planes. Moreover, taking into account the aforementioned reaction mechanism and the related r.d.s. (4), it follows that on the MPF 12-8 sample the slow conversion of the C($s_{n-4}$) intermediate species into CO($s$) gives rise to a continuous accumulation of coke precursor in the form of surface carbide species, causing an initial slight decrease in activity. Thereafter, the progressive growth in the $C/Ni_s$ ratio entails the formation of carbon multilayers (*48*) which drastically limit the Ni accessibility and lead to the observed sudden drop in the catalytic activity. By contrast, the more regular morphology of larger Ni particles in MPF 12-std and MPF 12-6 catalysts allows a more effective removal of the C($s_{n-4}$) intermediate, rendering the Ni/MgO system significantly more stable against coke deposition.

## CONCLUSIONS

Ni/MgO is both active and stable as a catalyst for the steam reforming of methane. The results presented show that:

(i) high calcination temperatures (>600°C) and low Ni loadings (<11.0%) promote the formation of unreducible NiO–MgO solid solution (*1*), limiting the suitability of Ni/MgO as a real $CH_4$ steam reforming catalyst;

(ii) both the metal surface area and the catalytic activity depend on the reduction temperature according to a volcano-shape relationship;

(iii) high metal dispersions (>15%) negatively affect both the activity and the stability of Ni/MgO, providing evidence for the *structure-sensitive* character of the methane steam reforming reaction.

## REFERENCES

1. Arena, F., Horrell, B. A., Cocke, D. L., Parmaliana, A., and Giordano, N., *J. Catal.* **132,** 58 (1991).
2. Borowiecki, T., *Appl. Catal.* **10,** 273 (1984).
3. Hagan, A. P., Lofthouse, M. G., Stone, F. S., and Trevethan, M. A., *in* "Preparation of Catalysts II" (B. Delmon, P. Grange, P. A. Jacobs, and G. Poncelet, Eds.), p. 417. Elsevier, Amsterdam, 1979.
4. Highfield, J. G., Bossi, A., and Stone, F. S., *in* "Preparation of Catalysts III" (G. Poncelet, P. Grange, and P. A. Jacobs, Eds.), p. 181. Elsevier, Amsterdam, 1983.

5. Zecchina, A., Spoto, G., Coluccia, S., and Guglielminotti, E., *J. Chem. Soc. Faraday Trans. 1* **80,** 1891 (1984).
6. Takezawa, N., Terenuma, H., Shimokawabe, M., and Kobayashi, H., *Appl. Catal.* **23,** 291 (1986).
7. Borowiecki, T., *Appl. Catal.* **4,** 223 (1982).
8. Cimino, A., Gazzoli, D., Indovina, V., Inversi, M., Moretti, G., and Occhiuzzi, M., *in* "Structure and Reactivity of Surfaces" (C. Morterra, A. Zecchina, and G. Costa, Eds.) p. 181. Elsevier, Amsterdam, 1989.
9. Parmaliana, A., Frusteri, F., Arena, F., Mondello, N., and Giordano, N., *in* "Structure and Reactivity of Surfaces" (C. Morterra, A. Zecchina, and G. Costa, Eds.) p. 739. Elsevier, Amsterdam, 1989.
10. Bond, G. C., and Sarsam, S. P., *Appl. Catal.* **38,** 365 (1988).
11. Parmaliana, A., Arena, F., Frusteri, F., and Giordano, N., *J. Chem. Soc. Faraday Trans.* **86,** 2663 (1990).
12. Arena, F., Licciardello, A., and Parmaliana, A., *Catal. Lett.* **6,** 121 (1990).
13. Maubert, A., Martin, G. A., Praliaud, H., and Turlier, P., *React. Kinet. Catal. Lett.* **22,** 203 (1983).
14. Borowiecki, T., *Appl. Catal.* **31,** 207 (1987).
15. Rostrup-Nielsen, J. R., *in* "Steam Reforming Catalysts." Danish Technical Press, Copenhagen, 1975.
16. Borowiecki, T., *React. Kinet. Catal. Lett.* **33,** 429 (1987).
17. Holt, T. E., Logan, A. D., Chakaraborti, S., and Datye, A. K., *Appl. Catal.* **34,** 199 (1987).
18. Narayanan, S., and Sreekanth, G., *J. Chem. Soc. Faraday Trans. 1* **85**(11), 3785 (1989).
19. Matsuura, I., Hashimoto, Y., Takayasu, O., Nitta, K., and Yoshida, Y., *Appl. Catal.* **74,** 273 (1991).
20. Delannay, F., *in* "Characterization of Heterogeneous Catalysts." Dekker, New York, 1984.
21. Eischens, R. P., Pliskin, W. A., and Francis, S. A., *J. Chem. Phys.* **22,** 1786 (1954); Eischens, R. P., Francis, S. A., and Pliskin, W. A., *J. Phys. Chem.* **60,** 194 (1965); Eischens, R. P., and Pliskin, W. A., *in* "Advances in Catalysis" (D. D. Eley, H. Pines, and P. B. Weisz, Eds.), Vol. 10, p. 1, Academic Press, New York, 1958.
22. Sheppard, N., and Nguyen, T. T., *in* "Advances in Infrared and Raman Spectroscopy" (P. J. Clarke, and R. E. Hester, Eds.), Vol. 4, p. 67. Wiley, New York, 1978, and references therein.
23. Blyholder, G., and Bowen, D. O., *J. Phys. Chem.* **66,** 1288 (1962).
24. Primet, M., Dalmon, J. A., and Martin, G. A., *J. Catal.* **46,** 25 (1977); Dalmon, J. A., Primet, M., Martin, G. A., and Imelik, B., *Surf. Sci.* **50,** 95 (1975).
25. Mirodatos, C., Praliaud, H., and Primet, M., *J. Catal.* **107,** 275 (1987).
26. Rochester, C. H., and Terrel, R. J., *J. Chem. Soc. Faraday Trans. 1* **73,** 609 (1977).
27. Bartholomew, C. H., and Pannell, R. B., *J. Catal.* **65,** 390 (1980).
28. Blackmond, D. G., and Ko, E. I., *J. Catal.* **96,** 210 (1985).
29. Ciocco, M. V., and Blackmond, D. G., *Appl. Catal.* **44,** 105 (1988).
30. Little, L. H., "Infrared Spectra of Adsorbed Species." Academic Press, New York, 1966.
31. Mohana Rao, K., Scarano, D., Spoto, G., and Zecchina, A., *Surf. Sci.* **204,** 319 (1988).
32. Galuszka, J., Chang, J. R., and Amenomiya, Y., *J. Catal.* **68,** 172 (1981).
33. Chiorino, A., Garrone, E., Ghiotti, G., Guglielminotti, E., and Zecchina, A., *in* "Proceedings, 7th International Congress on Catalysis, Tokyo, 1980" (T. Seiyama, and K. Tanabe, Eds.), p. 136. Elsevier, Amsterdam, 1981.
34. Guglielminotti, E., Zecchina, A., Boccuzzi, F., and Borrello, E., *in* "Growth and Properties of Metal Clusters" (J. Bourdon, Ed.), p. 165. Elsevier, Amsterdam, 1980.
35. Louis, C., Marchese, L., Coluccia, S., and Zecchina, A., *J. Chem. Soc. Faraday Trans. 1* **85,** 1655 (1989).
36. Shen, W. M., Dumesic, J. A., and Hill Jr., C. G., *J. Catal.* **68,** 152 (1981).
37. Kipnis, A. Ya., and Michailova, N. F., *Zh. Prikl. Khim.* **45,** 1450 (1972).
38. Rostrup-Nielsen, J. R., *in* "Catalysis" (J. R. Anderson, and M. Bouduart, Eds.), Vol. 5, p. 1. Springer-Verlag, Berlin, 1984.
39. Che, M., and Bennett, C. O., *in* "Advances in Catalysis" (D. D. Eley, H. Pines, and P. B. Weisz, Eds.), Vol. 36, p. 55. Academic Press, San Diego, 1989.
40. Van Hardeveld, R., and Hartog, F., *in* "Advances in Catalysis" (D. D. Eley, H. Pines, and P. B. Weisz, Eds.), Vol. 23, p. 75. Academic Press, New York, 1972.
41. Leach, H. F., Mirodatos, C., and Whan, D. A., *J. Catal.* **63,** 138 (1980).
42. Agnelli, M. E., Ponzi, E. N., and Yeramian, A. A., *Ind. Eng. Chem. Res.* **26,** 1704 (1987).
43. Briot, P., Auroux, A., Jones, D., and Primet, M., *Appl. Catal.* **59,** 141 (1990).
44. Hicks, R. F., Qi, H., Young, M. L., and Lee, R. G., *J. Catal.* **122,** 280 (1990).
45. Doering, D. L., Dickinson, J. T., and Poppa, H., *J. Catal.* **73,** 91 (1982).
46. Arena, F., Parmaliana, A., Mondello, N., Frusteri, F., and Giordano, N., *Langmuir* **7,** 1555 (1991).
47. Bartholomew, C. H., *Catal. Rev.-Sci. Eng.* **24**(1), 67 (1982).
48. Duprez, D., Demicheli, M. C., Marecot, P., Barbier, J., Ferretti, O. A., and Ponzi, E. N., *J. Catal.* **124,** 324 (1990).